Defence Science Journal, Vol. 66, No. 4, July 2016, pp. 391-402, DOI : 10.14429/dsj.66.10214

RESEARCH PAPER

Effect of Mn Concentration on Magneto-mechnaical Properties in Directionally Solidified Ferromagnetic Shape Memory Ni-Mn-Ga Alloys

R.K Singh*, M. Manivel Raja, P. Ghosal, and R.P. Mathur

Defence Metallurgical Research Laboratory, Hyderabad - 500 058, India
**E-mail: ranjan@dmrl.drdo.in*

ABSTRACT

Heusler type alloys $Ni_{50}Mn_{25+x}Ga_{25-x}$ (x = 2, 3, 4, and 5) based on near stoichiometric Ni_2MnGa compositions were directionally solidified using modified Bridgman method. The alloys thus prepared were characterised for their chemical composition, crystal structure, microstructure, phase transformation, magnetic and magneto-mechanical properties. The directionally solidified $Ni_{50}Mn_{30}Ga_{20}$ alloy rod exhibited maximum magnetocrystalline value of 95 kJm^{-3} and lowest detwinning stresses for martensite phase of about 5 MPa. The reversible room temperature magnetic field induced strain of 0.2 per cent under external magnetic field of 0.6 T and 0.05 kN bias load was obtained for the directionally solidified $Ni_{50}Mn_{30}Ga_{20}$ alloy.

Keywords: Ferromagnetic shape memory alloys, directional solidification, martensitic transformation, magnetic field induced strains

1. INTRODUCTION

Ferromagnetic shape memory alloys (FMSAs) are relatively new class of active materials exhibiting large strains (up to 10 per cent) under an external magnetic field[1-5]. The phenomenon of ferromagnetic shape memory (FMSM) is explained on the basis that twin variants of the martensitic phase are reoriented by the application of magnetic field[6-10]. Due to redistribution of the martensite twin variants a large strain is attained without any change in the external temperature. This strain can be made reversible by either the application of compressive stress or magnetic field in a direction perpendicular to the original applied magnetic field. The essential material characteristics for the occurrence of the FMSM phenomenon is the ferromagnetic martensite phase having low detwinning stress and strong magnetocrystalline anisotropy[11,12]. Several alloy systems viz. Fe-Pt, Fe-Pd, Ni-Mn-Ga, Ni-Mn-Al, Ni-Fe-Ga, Co-Ni-Al, Co-Ni-Ga *etc.*[13,14] exhibit this phenomenon, however Ni-Mn-Ga system has gained considerable importance in recent years due to its large values of magnetic field induced strains (MFIS) at room temperature. Among the different classes of active materials like magnetostrictive, piezoelectric and conventional shape memory, each class has its advantages and drawbacks and therefore its own area of application. While the magnetostrictive and piezoelectric materials have a faster response frequency, its recoverable strains are small. On the other hand, the shape memory materials exhibit large recoverable strains but its response frequency is slow due to the relatively slow heating and cooling process. The magnetically driven FMSAs, in particular the Ni-Mn-Ga alloys provide an optimum combination of large recoverable strains at faster response frequency making them highly interesting for many technological applications such as actuators and sensors[15]. The prominent areas envisaged for the application of FMSAs includes stroke delivery applications (actuators), energy applications, active damping control, bio-medical, etc.

The strains induced by magnetic field in FMSAs are two orders of magnitude greater than that in magnetostrictive materials and are equivalent to that observed in SMAs. Also, magnetostriction is observed in structurally homogeneous samples, whereas the FMSM effect requires a special microstructure. This microstructure is provided by a martensitic transformation. Similar to that in shape memory alloys, the different variants of the martensite are twin related to each other with well-defined twin boundary between them in FMSAs. However, the fundamental difference between a martensite phase of conventional shape memory and ferromagnetic shape memory alloys is its ferromagnetic nature. This additional (magnetic) degree of freedom in FMSAs allows the twin boundaries between two martensite variants to move on application of an external magnetic field. The driving force for the movement of twin boundaries is the orientation of the spontaneous magnetic moment or the magnetocrystalline anisotropy. Magnetic materials such as ferromagnets, antiferromagnets and ferrimagnets are characterised by spontaneous magnetisation. In the absence of an external magnetic field their magnetisation has a certain preferable direction with respect to the crystal lattice, the so-called easy direction. In a twinned microstructure the lattice orientations of the twin variants are different and therefore the magnetisation directions also differ.When an external magnetic field is applied, the magnetic moments try to align with the field. If the energy needed to rotate the magnetisation away

Received : 21 March 2016, Revised : 26 April 2016
Accepted : 02 June 2016, Online published : 28 June 2016

from the easy direction (i.e. the magnetic anisotropy energy) is high enough, it may be energetically favourable to move the twin boundaries instead. Also, the detwinning stresses of the martensite phase should be low so that it can be overcome by the magnetic stresses generated at the twin boundaries. Under favourable conditions, the fraction of twins with the easy axis in the direction of the field will grow at the expense of the other twin variants by the application of magnetic field. This process results in large shape changes and the phenomenon is called ferromagnetic shape memory effect. The magnetic field induced strains are reversible on application of magnetic field or stress in direction perpendicular to the originally applied magnetic field direction.

The reversible strain output depends on the applied magnetic field and compressive pre-stress level applied to the sample. With increase in compressive pre-stress the magnetic field induced strain decreases because of the blocking force. It can also be seen in the figure, that strain path during increase and decrease in magnetic fields show hysteresis. This indicates excellent damping capabilities of the Ni-Mn-Ga alloys. From the materials point of view, the basic requirements for appearance of the FMSM effect can be summarised as

(i) ferromagnetic martensite phase
(ii) strong magnetic anisotropy energy to avoid magnetisation flips, and
(iii) low twinning stresses of the martensite phase.

In Ni-Mn-Ga alloys the martensite transformation temperature is strongly dependent on the composition. In the stoichiometric Heusler Ni_2MnGa alloy, the martensitic transformation occurs at 200 K leading to a modulated tetragonal martensite with lattice parameters $a = b = 0.5920$ nm and $c = 0.5566$ nm[17]. However, systematic studies on this alloy system have shown that the off-stoichiometric composition can have transformation temperatures well above the room temperature. An empirical dependence of the martensite transformation temperature (T_M) on the average electron concentration per atom (*e/a* ratio) was established[18], according to which T_M increases with increase in *e/a* ratio of the alloy. The high temperature austenite phase in the Ni-Mn-Ga alloys is cubic with an $L2_1$ order belonging to space group Fm-3m (No 225). Depending mainly on the alloy composition this high temperature phase transforms to either nonmodulated tetragonal structure or to modulated martensite structure[19,20]. The nonmodulated tetragonal structure (space group I4/mmm, No 139) is the most stable one among the different Ni-Mn-Ga martensite phases[21]. The alloys transforming straight from the parent to this non-modulated tetragonal structure phase have typical transformation temperatures close or above the Curie point[22]. The modulated martensite structure transforms directly from the parent phase at lower temperatures close to the ambient and usually below the Curie point[23]. In general, based on the period of modulation *i.e.* five planes or seven planes, these structures are called as 5 M and 7 M martensite respectively. From the X-ray diffraction technique, the basic unit cell of the 5 M or 7 M martensite has been reported to be monoclinic and the modulation can be commensurate or incommensurate depending on the alloy composition.

The magnetic properties such as Curie temperature, saturation magnetisation, magnetocrystalline anisotropy are essential requirements for the ferromagnetic shape memory alloys. In Ni-Mn-Ga alloys the T_C is less sensitive to composition (*e/a* ratio) as compared to martensite transformation temperature[1]. Therefore, T_C cannot be increased much by composition variation which limits the service temperature of the Ni-Mn-Ga ferromagnetic shape memory alloys. The reported value of T_C for stoichiometric (Ni_2MnGa) composition is 376 K[24]. The magnetic moment of Ni-Mn-Ga alloys originates mainly from Mn atoms having the largest magnetic moment, while the Ni atoms possess small magnetic moments. However, by increasing the Mn concentration both the saturation magnetisation and T_C decreases. This decrease in ferromagnetic properties is due to the antiferromagnetic coupling of the excess Mn atoms with the neighbouring Mn atoms[25].

Another very important magnetic property responsible for the FMSM effect is the magnetocrystalline anisotropy. Measurements of magnetisation in austenite phase of single crystal have shown that the easy magnetisation axis in the cubic phase is oriented along the crystallographic [100] axis and that the magnetocrystalline anisotropy constant K_1 in this phase is relatively moderate[26]. However, in martensite state the magnetocrystalline anisotropy varies significantly with the crystal structure. Studies of the magnetocrystalline anisotropy of singlecrystals $Ni_{2+x+y}Mn_{1-x}Ga_{1-y}$ of different compositions in single-variant state have shown that the values of uniaxial anisotropy constant (K_u) at room temperature vary from 1.7×10^6 ergcm^{-3} for $Ni_{48}Mn_{31}Ga_{21}$ [27] to 2.48×10^6 ergcm^{-3} for $Ni_{49.7}Mn_{28.7}Mn_{21.6}$ [71]. In martensite phase usually the shorter axis of the unit cell is the easy axis of the magnetisation. In modulated martensite phase *c/a* is less than 1, therefore *c* axis is the easy axis of the magnetisation while in non-modulated martensite phase it is *a* axis[28].

The Ni-Mn-Ga alloys belong to the most important class of FMSM materials and these alloys have been extensively studied in single crystalline and polycrystalline forms for their structural transformation, crystal structures, atomic ordering, magnetic properties, and magnetic field induced strains and related other aspects. Unfortunately, till date the large magnetic field induced strains have been reported in single crystals which are difficult to prepare and expensive. In polycrystalline state Ni-Mn-Ga alloys exhibit poor mechanical properties and are extremely brittle. Considering the technological importance of the oriented polycrystalline alloys, it is proposed to carry out directional solidification of Mn rich Ni-Mn-Ga alloys with nominal composition: $Ni_{50}Mn_{25+x}Ga_{25-x}$ (where x = 2, 3, 4, 5 at%) and to evaluate its FMSM related properties in this study.

2. EXPERIMENTAL WORK

The alloy designation, nominal compositions along with crystal growth conditions are given in Table 1. The above alloys were prepared using high purity elements *viz.* 99.9 % Mn, 99.99 % Ni, and 99.9999 % Ga in a vacuum induction melting furnace under Argon atmosphere. Roughly 3 wt% excess Mn was added in every charge in order to compensate for the Mn losses during melting.

Table 1. Designations, nominal compositions, and growth conditions of directionally solidified alloys

Alloy Designation ($Ni_{50}Mn_{25+x}Ga_{25-x}$)	Nominal Composition (at%)	Temperature gradient (K mm^{-1})	Holding Temperature (K)	Withdrawal rates (cm h^{-1})
x = 2	$Ni_{50}Mn_{27}Ga_{23}$	10	1623	10
x = 3	$Ni_{50}Mn_{28}Ga_{22}$	10	1623	10
x = 4	$Ni_{50}Mn_{29}Ga_{21}$	10	1623	10
x = 5	$Ni_{50}Mn_{30}Ga_{20}$	10	1623	10

The resulting molten alloys were chill cast into ceramic alumina tubes (inner diameter 10 mm) mounted on a water cooled Cu chill plate. Typical chill cast precursor rod for directional solidification and its optical micrograph of the longitudinal section are shown in Fig. 1(a)-(b). Fine columnar grain structure is clearly observed at the bottom of the chill cast rods. These oriented grains act as seed during the directional solidification. The directional solidification of these rods was carried out using a modified Bridgman method, in which ceramic alumina crucible containing the molten alloy is pulled through a temperature gradient. A two-zone directional solidification furnace with a fixed temperature gradient of 10 K mm^{-1} was used for directional solidification. For the characterisation of the directionally solidified rods, 5 mm portion from the top and bottom of the rods were discarded and samples were taken from the remaining portion of the rods for studies.

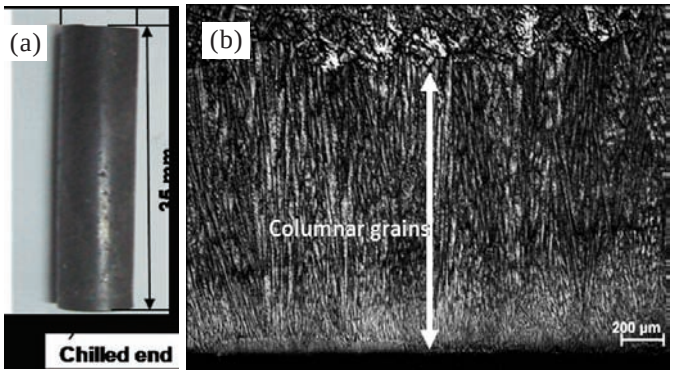

Figure 1. (a) A typical bottom chill cast precursor rod for directional solidification, and (b) optical micrograph of longitudinal section of the bottom chill cast rods.

3. RESULTS AND DISCUSSION

3.1 Microstructural Features

The microstructures of transverse section of the directionally solidified Mn-rich $Ni_{50}Mn_{25+x}Ga_{25-x}$ (at%, where x = 2, 3, 4, 5) Heusler type alloys, prepared under identical growth conditions are shown in Fig. 2. Under the employed growth conditions, the microstructures of transverse section indicate a cellular kind of solidification morphology. The grain in millimeter range consists of subgrain cells of about 250 µm. The transverse grain boundaries are omitted during

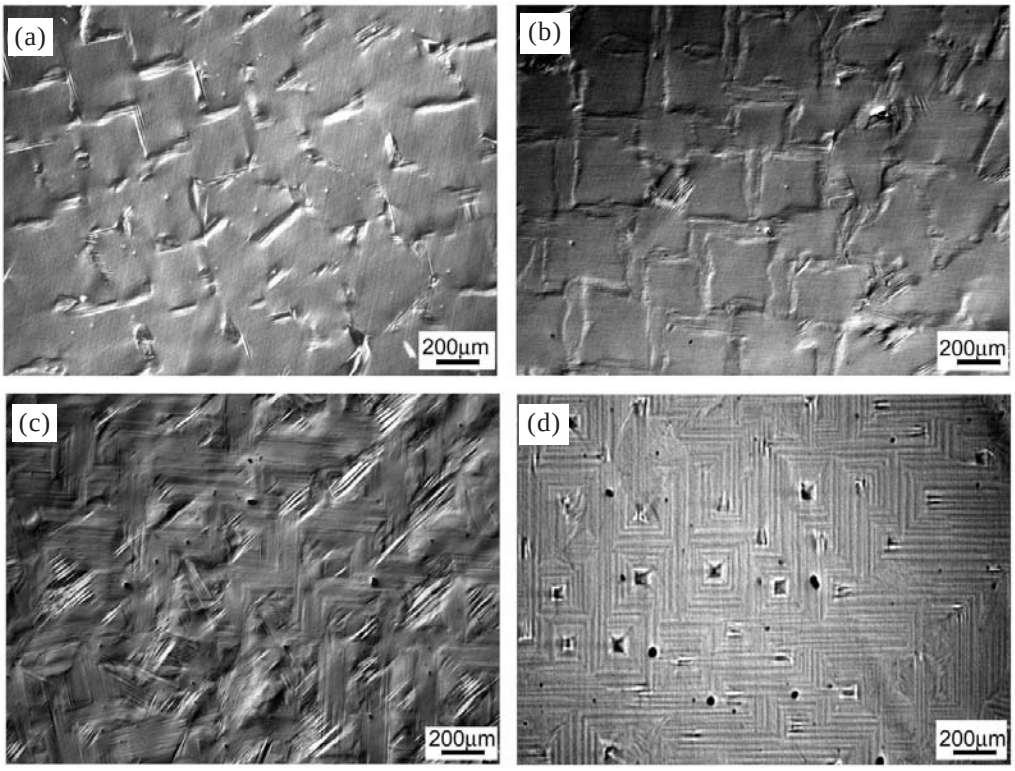

Figure 2. Optical micrograph of the transverse section of directionally solidified $Ni_{50}Mn_{25+x}Ga_{25-x}$ alloys with (a) x = 2, (b) x = 3, (c) x = 4, and (d) x = 5.

directional solidification because the elongated grains grow freely into the melt and do not impinge on other grains. Since the crystal growth conditions are identical, the variant chemical composition of the alloys does not affect the cell or grain size. However, it greatly influences the microstructural features inside the cell. Fig. 3 shows the typical micrograph of the subgrain structure at higher magnification for the alloy having lowest (Fig. 3(a)) and highest Mn content (Fig. 3(b)) in the present study. Three distinct regions can be clearly identified in each micrograph and are marked as region A, B, and C. The regions A and B consist of martensite twin variants having straight and curved twin boundaries respectively, whereas no martensite twin variants are observed in region C. The volume fraction of region C decreases and of region A /B increases as the Mn content increases. This feature of the microstructure suggests that the cell center (region C) consists of austenite phase whereas the martensite phase preferentially nucleates at the cell boundaries.

The optical micrographs of longitudinal section of the directionally solidified rods are shown in Fig. 4. It clearly indicates a cellular kind of solidification morphology in which the martensite phase prefers to nucleate at cell boundaries as a result of chemical segregation. Irrespective of alloy composition the cells are aligned in the growth direction. However, as the Mn concentration in the alloy increases, a continuous distribution of martensite plates is seen at the cell boundaries. Also, the martensite plate thickness decreases with the increase in the Mn content. Interestingly, the martensite plates cannot be seen inside the cell matrix which is in accordance with the transverse microstructure. The solid-liquid interface during directional solidification can be planar, cellular or dendritic. The cellular structure which forms just above the threshold conditions of

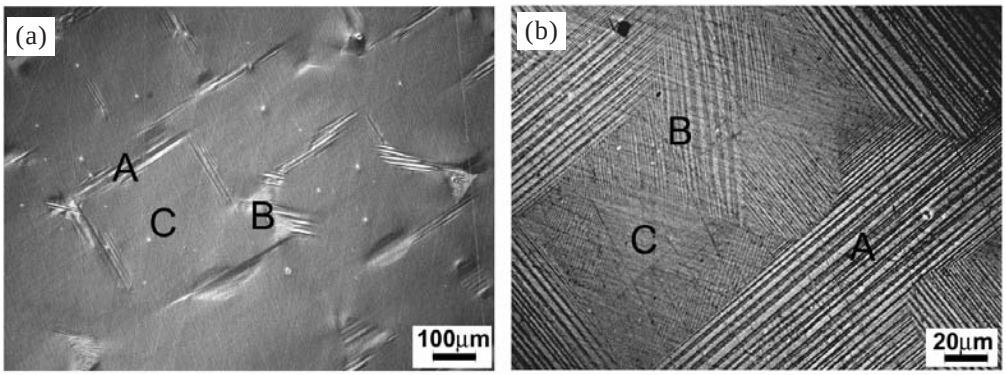

Figure 3. Optical micrograph of the transverse section of directionally solidified $Ni_{50}Mn_{25+x}Ga_{25-x}$ alloys with (a) x = 2 and (b) x = 5 at higher magnification.

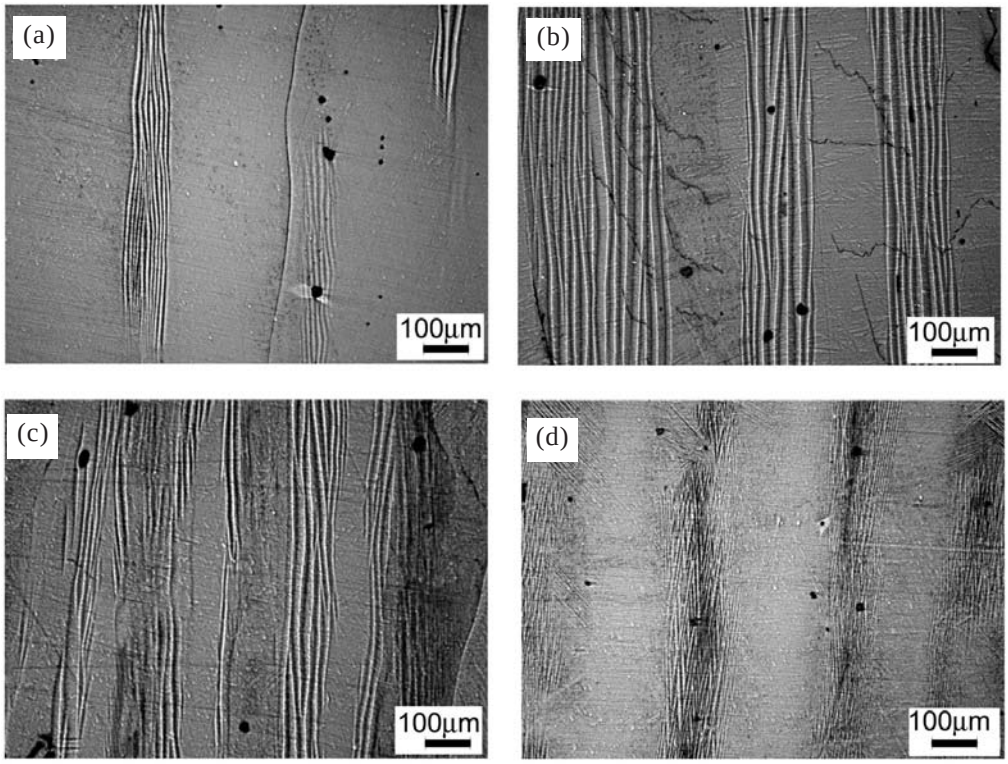

Figure 4. Optical micrograph of the longitudinal section of directionally solidified $Ni_{50}Mn_{25+x}Ga_{25-x}$ alloys with (a) x = 2, (b) x = 3, (c) x = 4 and (d) x = 5.

planar interface stability has two important characteristics. First, the length of the cell is very small, and it is of the same order of magnitude as the cell spacing. Second, the tip region of the cell is broader and the cell has a larger tip radius. Thus a significant solute buildup occurs ahead of the interface with some solute diffusing in the lateral directions[29]. In the present study, the growth conditions employed are well beyond the threshold conditions of planar interface stability. In this case, the cell tip becomes sharper and assumes a nearly parabolic shape which is somewhat similar to the dendritic tip shape. Also, length of the cell increases, and this kind of solidification morphology is termed as cellular-dendritic[30-32]. As the cell tip becomes sharper, more solute transport occurs laterally so that the intercellular region becomes richer in solute giving rise to microsegregation patterns in the solidified materials. The microsegregation pattern of solutes has been studied by EPMA. Table 2 lists the composition of the directionally solidified rods at the cell center (region C) and at the cell boundaries (region A/B) in transverse section of the rods.

From Table 2 it is evident that there is significant transport of solute in the lateral direction. The microsegregation effect is generally characterised by the segregation ratio (SR) which is defined as the ratio of the maximum solid composition (at the cell base) to the minimum solid composition (at the cell tip)[33]. In a transverse section, SR is the ratio of solute concentration at the cell boundary and at the cell center. The variation of SR for each element as a function of nominal Mn content is shown in Fig. 5. It can be seen that with the increase in the Mn content, the cell center gets enriched in Ga content whereas cell boundaries are enriched in Mn content. Since the nominal composition of Ni is not changed in the alloys its SR do not change with the variation in nominal composition of Mn. However, SR value of Ni indicates that the cell center is slightly enriched in Ni content.

3.2 Martensite Transformation and Magnetic Properties

The influence of directional solidification on the martensitic transformation temperatures has been studied by differential scanning calorimetry (DSC). Figure 6(a) shows the DSC thermograms of the $Ni_{50}Mn_{25+x}Ga_{25-x}$ (x = 2, 3, 4, 5) alloys in induction melted and chill-cast condition. The first order peaks corresponding to forward and reverse martensite transformations during cooling and heating are clearly observed in the DSC thermograms. The corresponding martensite start (T_{Ms}) and finish (T_{Mf}) during cooling and austenite start (T_{As}) and finish (T_{Af}) during heating, were determined by the tangent

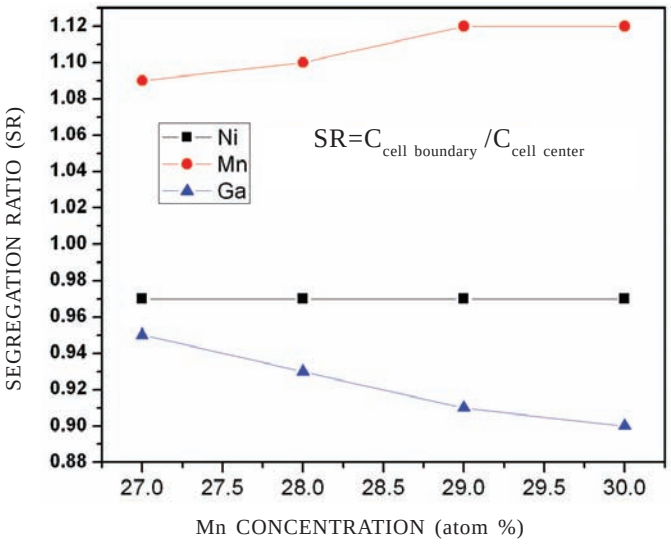

Figure 5. Segregation ratio of directionally solidified $Ni_{50}Mn_{25+x}Ga_{25-x}$ alloys as a function of Mn content.

intersection method from the onset of the DSC peaks. The martensitic transformation temperature (T_M) was calculated using the relation $T_M = (M_s + A_f)/2$. The obtained values are summarised in Table 3. The Table shows that T_M increases with increase in the Mn substitution for Ga. In Ni-Mn-Ga alloys, it has been reported that the T_M value strongly depends on the valence electron concentration (*e/a*), which in turn depends on composition. In general, T_M increases with increase in the *e/a* ratio of the alloys. Considering the outermost electrons of the constituent elements [Ni- 10 ($3d^8 4s^2$), Mn - 7 ($3d^5 4s^2$) and Ga -3 ($4s^2 4p^1$)], the average electron concentration (*e/a*) can be expressed as follows

$$e/a = \frac{10x(Ni_{at\%}) + 7x(Mn_{at\%}) + 3x(Ga_{at\%})}{(Ni_{at\%} + Mn_{at\%} + Ga_{at\%})} \quad (1)$$

The *e/a* ratios calculated for different alloys using nominal composition and equation 1 listed in Table 3 demonstrate that the T_M value increases with increase in *e/a* ratio. It is well known that the martensitic transformation occurs when the Fermi surface touches the Brillouin zone boundary[17]. This situation implies that the change in the number of valence electrons and the modification of the Brillouin zone boundary can be considered to affect T_M in these Heusler alloys. In the present series of $Ni_{50}Mn_{25+x}Ga_{25-x}$ (x = 2, 3, 4, 5) alloys, increase of Mn substitution for Ga results in the increase of *e/a* ratio and thus causes the excess electrons above the Fermi level to move

Table 2. Compositional analysis of directionally solidified $Ni_{50}Mn_{25+x}Ga_{25-x}$ (x = 2, 3, 4, 5) alloys

Alloy (x)	Cell center (atom% ± std. dev.)			Cell boundaries (atom% ± std. dev.)		
	Ni	Mn	Ga	Ni	Mn	Ga
2	50.87 ± 0.31	26.79 ± 0.75	22.34 ± 0.52	49.61 ± 0.44	29.25 ± 0.85	21.14 ± 0.43
3	50.41 ± 0.22	28.27 ± 0.56	21.32 ± 0.55	49.03 ± 0.60	31.08 ± 0.54	19.89 ± 0.46
4	50.60 ± 0.52	28.64 ± 0.78	20.76 ± 0.48	48.87 ± 0.34	32.16 ± 0.25	18.97 ± 0.20
5	50.99 ± 0.27	29.12± 0.48	19.89 ± 0.38	49.56 ± 0.28	32.60 ± 0.54	17.84 ± 0.32

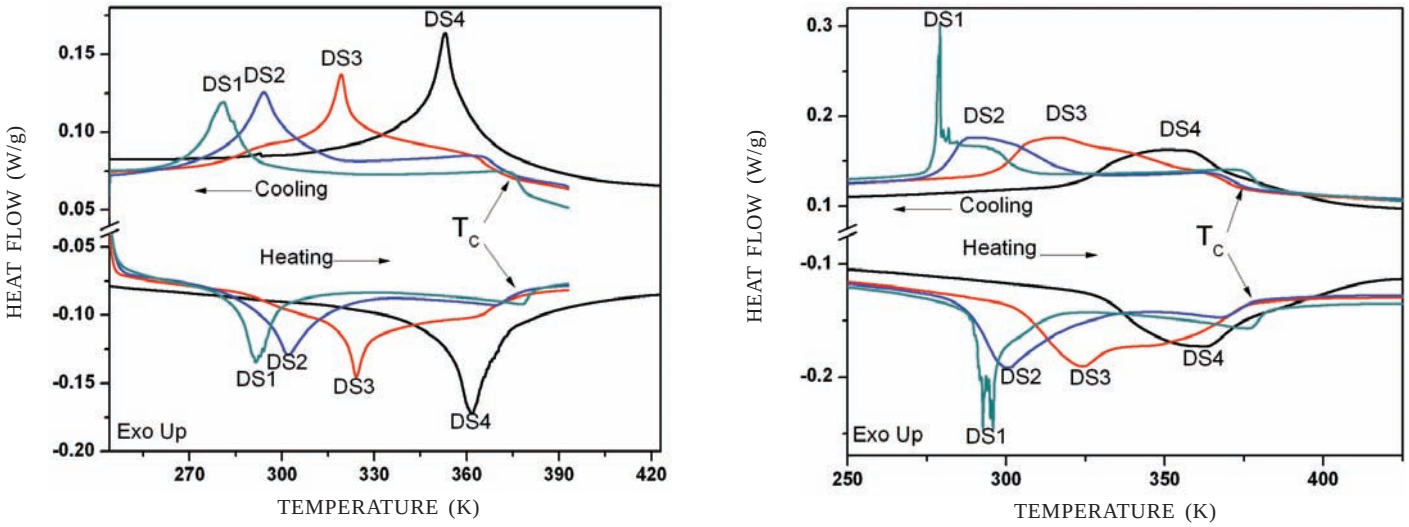

Figure 6. DSC thermograms of $Ni_{50}Mn_{25+x}Ga_{25-x}$ (x= 2, 3, 4, 5) alloys (a) after induction melting and chill-casting and (b) after directional solidification.

Table 3. Martensitic transformation temperature of $Ni_{50}Mn_{25+x}Ga_{25-x}$ (x= 2, 3, 4, 5) alloys after induction melting and chill-casting.

Alloy (x)	Martensite start (T_{Ms})	Martensite finish (T_{Mf})	Austenite start (T_{As})	Austenite finish (T_{Af})	$T_M = (T_{Ms} + T_{Af})/2$	e/a
2	291	270	285	300	295.5	7.58
3	313	283	289	319	316	7.62
4	324	313	319	330	327	7.66
5	374	338	344	380	377	7.70

to the corner states of the Brillouin zone. In this high energy state, the system undergoes a structural distortion of the lattice to minimise the total Gibbs free energy resulting in a more stable martensite structure. Thus the stability of martensite phase increases with increase in the *e/a* ratio.

Figure 6(b) shows the DSC thermograms of the $Ni_{50}Mn_{25+x}Ga_{25-x}$ (x = 2, 3, 4, 5) alloys after directional solidification. The DSC peaks appears to be broadened by directional solidification process and this broadening of the DSC peaks can be mainly attributed to the lateral microsegregation pattern of solutes.

From the EPMA it is known that cell boundaries get preferentially enriched in Mn while the cell center becomes Ga enriched. The *e/a* ratio of cell boundaries is higher than that at the cell center. This leads to a difference in martensitic transformation temperature at the cell center and boundaries, with latter transforming at higher temperature. This is in accordance with the observed optical microstructure (Fig. 3(a)-(b) taken at room temperature where in the regions A/B close to cell boundaries shows martensite phase while region C appears to be austenite phase. Also, with increase in average Mn content of the alloys, SR for Mn increases, so the martensite transformation width (M_s-M_f) increases as seen in Fig. 6(b).

In addition to the first order peaks in DSC thermograms, a second order kink (marked by arrow) can also be seen in Fig. 6 (a)-(b). This kink corresponds to the Curie temperature of the alloys. It may be noted in Fig. 6 that second order kink in $Ni_{50}Mn_{30}Ga_{20}$ (at%) alloy is not observed. This is attributed to the overlapping of the martensitic and Curie transition temperatures at this composition[34]. The Curie temperature of the directionally solidified alloys was also determined by measuring magnetisation as a function of temperature (thermomagnetic measurement) at a constant magnetic field of 500 Oe. The temperature was controlled with in an accuracy of ± 1 K using a variable temperature cryostat attached with VSM. The magnetisation data were collected during heating cycle at an interval of 3 K min^{-1} over a large temperature range. The thermomagnetic graphs for the directionally solidified alloys are shown in Fig. 7(a). The Curie temperature for an alloy was approximated by taking the high temperature inflection point in the thermomagnetic curve. From the Fig. 7(a) it is evident that the Curie temperature decreases with the increase in Mn content of the alloys, which is in accordance with the reported trend in Mn-rich Ni-Mn-Ga alloys[35]. The highest Curie temperature is reported in the stoichiometric Ni_2MnGa. The observed decrease in Curie temperature is accounted for by antiferromagnetic coupling of the extra Mn atoms at Ga site with the Mn atoms at Mn site[35]. The room temperature hysteresis loops (M *vs* H) of directionally solidified alloys are shown in Fig 7(b). The room temperature saturation magnetisation values for $Ni_{50}Mn_{25+x}Ga_{25-x}$ alloys with x = 2, 3, 4, and 5 are 68.4 emu g^{-1}, 64.0 emu g^{-1}, 63.0 emu g^{-1}, and 55.0 emu g^{-1}, respectively. It is evident that with increase in the Mn content (x) of alloys the saturation magnetisation decreases, in accordance with the antiferromagnetic coupling of excess Mn. Also, from Fig. 7(a) it can be inferred that at Curie temperature there is sharp decrease in the magnetisation values indicating that chemical segregation during directional solidification has negligible effect on the magnetic transition.

This is for the reason that the Curie temperature is less sensitive to the alloy composition as compared to martensitic transformation. The observed rise in magnetisation values in thermomagnetic curves at low temperature is due to the

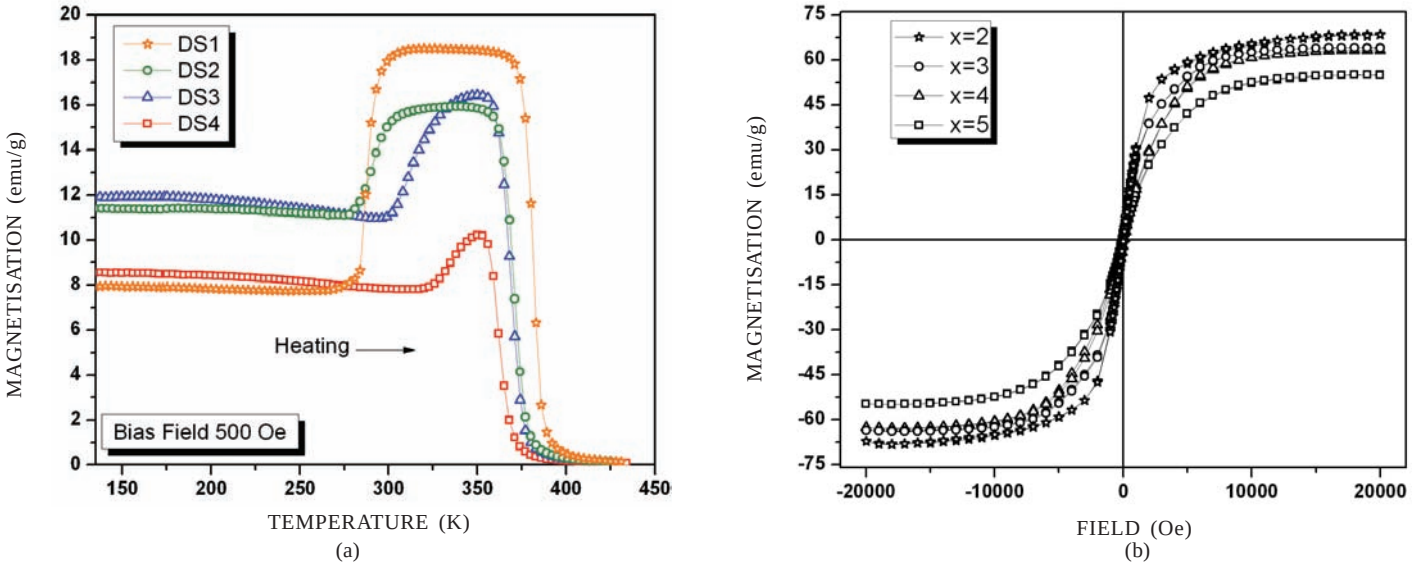

Figure 7. (a) Thermomagnetic curves and (b) hysteresis loop of directionally solidified $Ni_{50}Mn_{25+x}Ga_{25-x}$ (x= 2, 3, 4, 5) alloys.

reverse martensite to austenite transformation during heating. The reverse martensite to austenite temperatures approaches Curie temperature with increase in the Mn content of the alloys and at x = 5, the structural transformation merges with the Curie temperature. For the x = 2 alloy, the reverse martensitic transformation is just below the room temperature, accordingly the major phase should correspond to the austenite phase at room temperature. The room temperature coercivity values for $Ni_{50}Mn_{25+x}Ga_{25-x}$ alloys with x = 2, 3, 4, and 5 are 10 Oe, 101 Oe, 101 Oe, and 101 Oe respectively. An order less value of coercivity for the x = 2 alloy signifies that the relatively soft austenite phase is major phase in this alloy.

3.3 Crystal Structure at Room Temperature

The crystal structure of the phases present at room temperature was studied using x-ray diffraction (XRD) technique. The directionally solidified alloys were characterised in the bulk and powder form to study texture and crystal structure. The XRD patterns of the $Ni_{50}Mn_{25+x}Ga_{25-x}$ alloys, with x = 2, 3, 4, and 5, are shown in Fig. 8. The major phase in the x = 2 alloy is austenite (represented by A in Fig. 8) having $L2_1$ cubic crystal structure of $Fm\bar{3}m$ space group[17]. However, there are two additional peaks in powder XRD pattern of this alloy (marked by * in Fig. 8) that cannot be indexed in the austenite phase. On comparing the XRD patterns of alloys (with x = 2, 3, 4, and 5) in powder form in Fig. 8(b), the additional peaks can be assigned to the non-modulated martensite phase (represented by M in Fig. 8) with a space group of I4/mmm.

The volume fraction of austenite phase decreases while that of martensite phase increases with increase in Mn content (x value) of the alloys. This is evident from the relative decrease in intensity of the A(220) and A(422) peaks corresponding to the austenite phase. These results are in accordance with the DSC results confirming that martensite phase get stabilised by excess Mn content. On comparing the powder and bulk diffraction patterns of the x = 2 alloy, it is concluded that the A(220) and A(422) peaks are suppressed while the A(004) peak is enhanced after directional solidification. This difference in

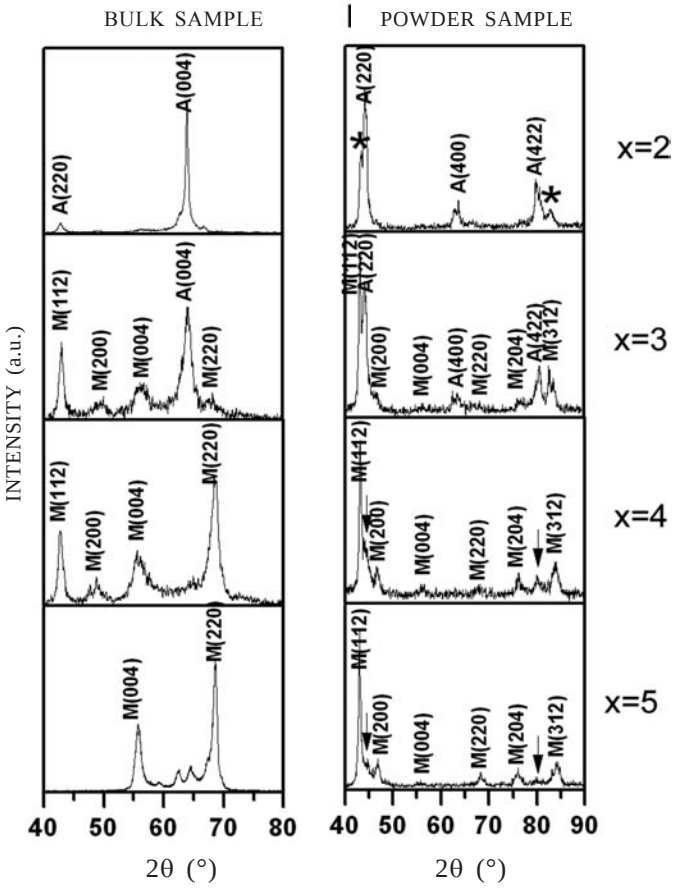

Figure 8. X-ray diffraction pattern of directionally solidified $Ni_{50}Mn_{25+x}Ga_{25-x}$ (x=2,3,4,5) alloys in (a) bulk and (b) powder forms. (A: austenite phase, M: Martensite phase).

the relative intensity of the bulk and powder diffraction patterns reveals the preferred grain growth direction during directional solidification is parallel to <100> crystallographic direction of the cubic austenite phase. In other alloys (x = 3, 4, 5), the relative intensity of M(220) and M(004) peaks gradually increases with

Mn content as evident from the complete suppression of low angle M(112) and M(200) peaks in the x = 5 alloy. These changes in relative intensities in bulk sample are closely related to the preferred selection of martensite variants in as grown condition. For the x = 5 alloy, the bulk XRD patterns exhibits some additional peaks between M(004) and M(220) that cannot be indexed by the non-modulated martensite structure. The origin of these peaks can be attributed either to the intermartensite phase or to the untransformed austenite phase as indicated by the powder XRD pattern of this alloy. Nonetheless, major phase in both the powder and bulk samples corresponds to the non-modulated martensite phase. The lattice parameters, martensite tetragonality and unit cell volumes of the constituent phases in the directionally solidified alloys were calculated from the powder XRD patterns and are summarised in Table 4. Shrinkage of the unit-cell volume for the austenite and martensite phase has been observed on incorporating excess Mn atoms for Ga. A decrease in the volume is expected as smaller size Mn atoms (covalent radius = 0.117 nm) is substituted for bigger Ga atoms (covalent radius = 0.1260 nm), provided the surplus Mn substitutes the Ga sites. The tetragonality of martensite phase is found to increase with the Mn content of the alloy. It is known that the high strength of austenite phase and the high tetragonality of BCT martensite phase seem to be favorable for reducing the twin thickness in martensite[36,37]. This leads to decrease in martensite twin thickness as observed for alloy with x = 5 in Fig. 4.

Table 4. The lattice parameters, tetragonality of martensite phase and unit cell volume of crystalline phases in $Ni_{50}Mn_{25+x}Ga_{25-x}$ (x = 2, 3, 4, 5) alloys

Alloy	Room temperature phase structure	Lattice parameters		Tetragonality (*c*/*a* ratio)	Unit cell volume (Å^3)
		a (Å)	*c* (Å)		
x = 2	Austenite	5.87	5.87	1	202.26
x = 3	Austenite ($L2_1$)	5.87	5.87	1	202.26
	Martensite (T)	3.94	6.50	1.64	100.90
x = 4	Austenite ($L2_1$)	5.83	5.83	1	198.15
	Martensite (T)	3.91	6.50	1.66	99.37
x = 5	Martensite (T)	3.90	6.56	1.68	99.77

3.3 Evaluation of Magneto-mechanical Properties

Room temperature compression test has been performed to study the deformation behaviour of the directionally solidified alloys in the as-grown state. The cylindrical axis of the samples was kept parallel to the growth direction. Fig. 9 shows the compressive stress-strain curves for the $Ni_{50}Mn_{25+x}Ga_{25-x}$ (x = 2, 3, 4, 5 at%) alloys. Different characteristic of compressive stress-strain curves were obtained for each alloy. For example, $Ni_{50}Mn_{25+x}Ga_{25-x}$ alloy with x = 2, only one stage is observed while in other alloys (x = 3, 4, 5) more than one deformation stages have been observed. Also, by measuring the initial and final dimensions of the sample it was found that the compressive deformation in the x = 2 alloy, was completely

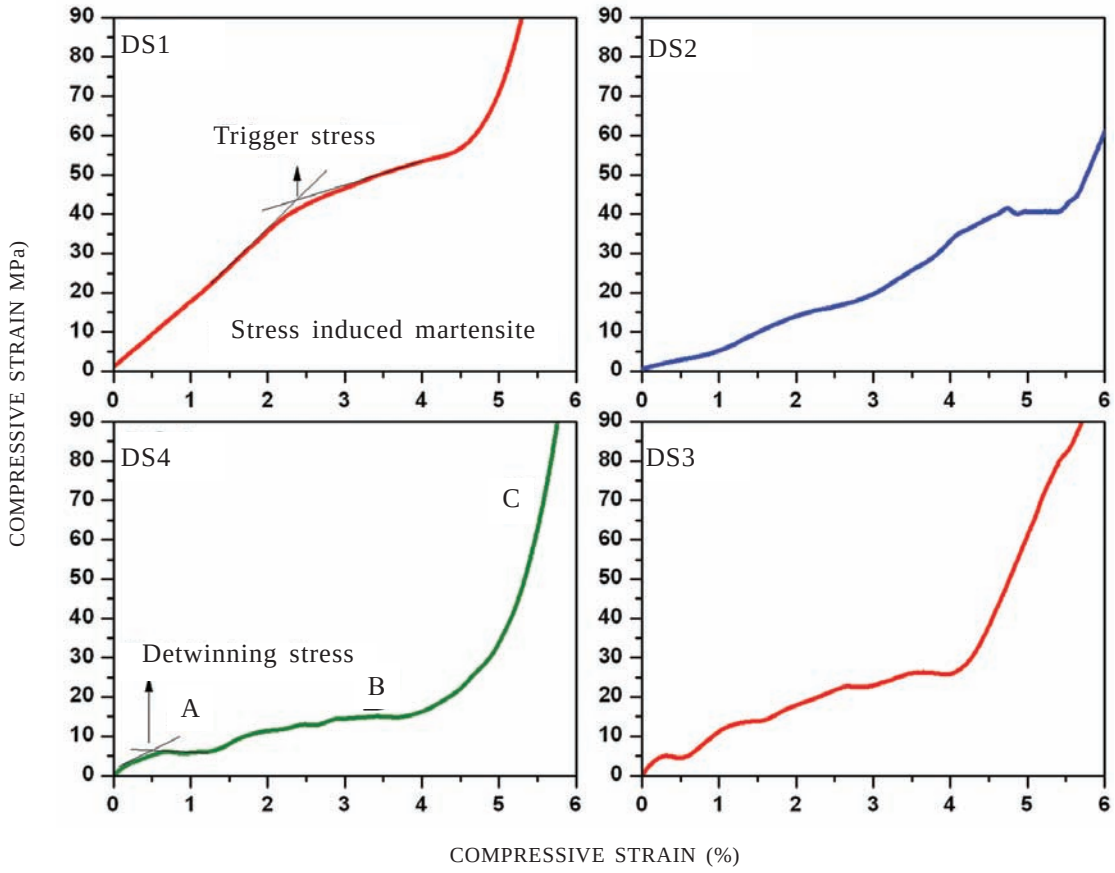

Figure 9. Room temperature compressive stress-strain curves for $Ni_{50}Mn_{25+x}Ga_{25-x}$ alloys (a) x = 2, (b) x = 3, (c) x = 4, and (d) x = 5.

reversible. The major room temperature phase in the x = 2 alloy is the austenite phase and the origin of single stage deformation can be related to the stress-induced martensite transformation[38]. The stress required to trigger stress-induced transformation was around 42 MPa, determined from the onset of stress plateau after the initial elastic deformation region. It is known that the martensite twin variants with their long axis (*c*-axis) perpendicular to the compressive directions are preferably generated during the stress-assisted martensitic transformations[39].

As Mn content (x value) increases in the $Ni_{50}Mn_{25+x}Ga_{25-x}$ alloys, the martensite phase get stabilised at room temperature and in alloy with x = 5, three distinct deformation stages, marked as region A, B, and C are clearly seen in Fig. 9(d). Regions A and B correspond mainly to the detwinning of martensite phase while region C is the elastic deformation of the detwinned martensite phase. It can be noticed that the region A has flat stress plateau while in region B the stress values increases at high strain. This can be attributed to the presence of untransformed austenite phase, observed in the powder XRD pattern. The detwinning stresses for martensite phase are about 5 MP in region A while in region B it varies from 10 MPa to 15 MPa. The low value of detwinning stresses in region A can be attributed to the presence of martensite twin variants with *c*-axis parallel to growth direction, resulting in twin planes approximately parallel to the maximum resolved shear stress plane. The compressive stress-strain curves of the remaining $Ni_{50}Mn_{25+x}Ga_{25-x}$ alloys with x = 3 and 4, indicate that the deformation initially proceeds by detwinning of martensite phase while at latter stage it proceeds by stress-induced martensite transformation. Interestingly, the total compressive strain remains constant, approximately 5 per cent for all the alloys.

After compression test the samples were further subjected to magnetisation measurement. The magnetisation curves measured in direction parallel and perpendicular to growth direction after compression are as shown in Fig. 10. The value of magnetic anisotropy constant, $|K_u|$ was estimated by the area enclosed by the two curves in Fig. 10. It can be seen that with increase in Mn content of alloys, the area enclosed by the two curves increases and for alloys with x = 4 and 5, calculated value of $|K_u|$ is about 52.26 kJm^{-3} and 95 kJm^{-3}. These values are less than that reported for non-modulated martensite phase (300 kJ m^{-3}) in Ni-Mn-Ga system[40] which can be attributed to the

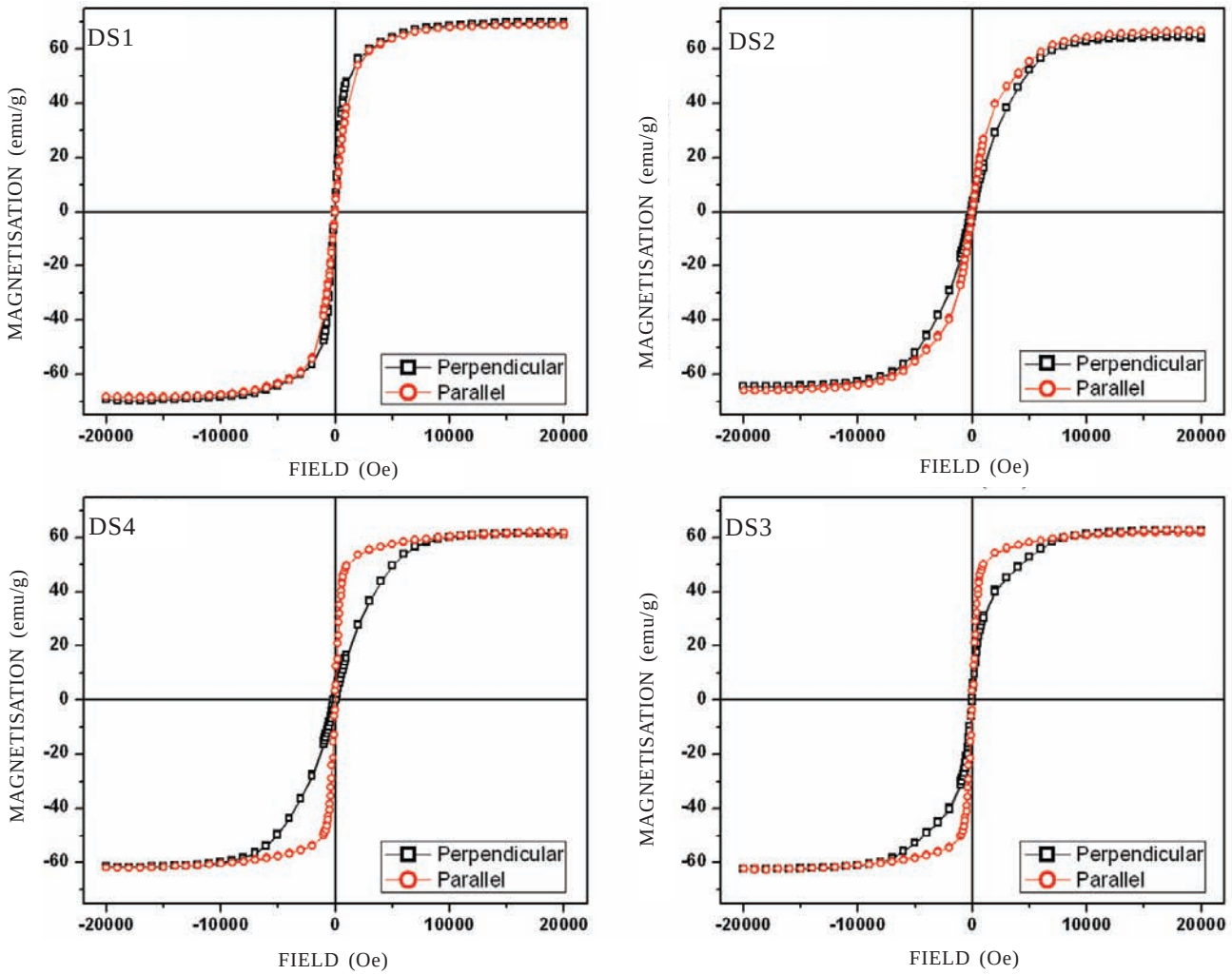

Figure 10. Room temperature magnetisation curves measured in direction parallel and perpendicular to the growth direction after compression of the directionally solidified $Ni_{50}Mn_{25+x}Ga_{25-x}$, a) x = 2, (b) x = 3, (c) x = 4, and (d) x = 5 alloys.

presence of untransformed austenite phase in the directionally solidified samples.

FMSM materials show reversible MFIS with external forces such as compressive stresses applied in transverse direction to the external magnetic fields. The MFIS measurement of FMSM alloys needs custom made magneto-mechanical test frame as no such ready built equipment is available. A preliminary system with a electromagnet was rigged up with mechanical test frame and the room temperature test were carried out on directionally solidified $Ni_{50}Mn_{25+x}Ga_{25-x}$ (x = 2, 3, 4, 5) alloys. In directionally solidified condition only $Ni_{50}Mn_{30}Ga_{20}$ alloy showed significant value of MFIS. The results obtained with this system for this alloy is shown in Fig. 11. Room temperature MFIS of 0.2 per cent under external magnetic field of 0.6 T and 0.05 kN external load was obtained for the directionally solidified $Ni_{50}Mn_{30}Ga_{20}$ alloy. On increasing the bias load to 0.1 kN the MFIS values dropped to 0.12 per cent. It may be noted that the obtained values are well below the values for single crystals however unlike polycrystalline state the low value of detwinning stress (5 MPa) and significant magnetocrystalline anisotropy (95 kJm^{-3}) enables Mn-rich directionally solidified rods to exhibit FMSM behaviour.

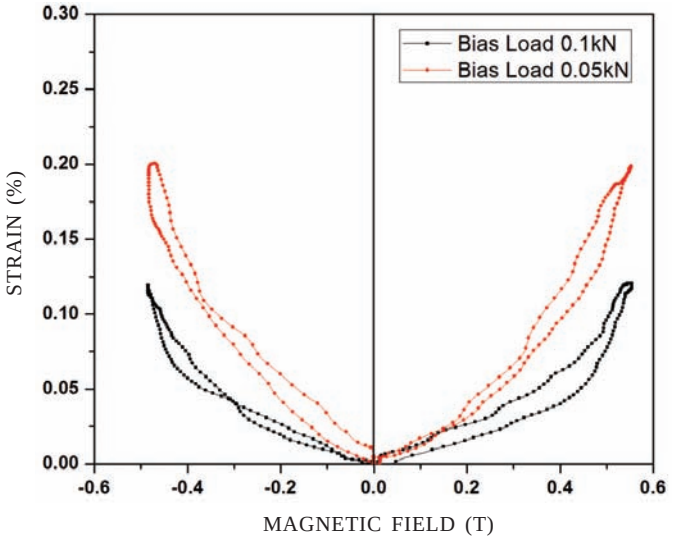

Figure 11. The reversible magnetic field induced strains in a directionally solidified $Ni_{50}Mn_{30}Ga_{20}$.

4. CONCLUSIONS

The directionally solidified rods of alloy series $Ni_{50}Mn_{25-x}Ga_{25+x}$ (2£x≤5) were prepared and the as-grown microstructure, texture, phases transformation temperatures, magnetic and mechanical properties were investigated in detail by various characterisation techniques. Under the employed growth conditions a cellular-dendritic kind of solidification morphology of the primary austenite phase was obtained.Significant lateral microsegregation of Mn and Ga is observed in cellular-dendritic solidification morphology. The segregation ratios for each element indicate that Mn has positive segregation tendency whereas Ga and Ni have negative segregation tendency indicating thereby that Mn is rejected into the liquid as the solidification progresses. As a result of lateral microsegregation, the martensite transformation temperature increases at cell boundaries and the DSC peaks become wider after directional solidification. On the whole, partial substitution of Mn for Ga in the Mn-rich $Ni_{50}Mn_{25+x}Ga_{25-x}$ (2 £ x ≤ 5) alloy series enhances the martensitic transformation temperatures. The magnetic properties such as Curie temperature and saturation magnetisation are less sensitive to the chemical segregation. The room temperature crystal structure changes from austenite to non-modulated martensite with increase in Mn concentration of the alloys. In cellular solidification morphology, the preferred grain growth direction was found to be approximately parallel to the <100> direction of the primary austenite phase. In as grown state presence of untransformed austenite phase has been noted even in alloys with martensite transformation temperature well above the room temperature. The volume fraction of untransformed austenite phase decreases with increase in the average Mn content in cellular-dendritic solidification morphology. The directionally solidified $Ni_{50}Mn_{30}Ga_{20}$ composition rod exhibited maximum magnetocrystalline value of 95 kJm^{-3} and detwinning stresses for martensite phase about 5 MPa. Room temperature reversible MFIS of 0.2 per cent under external magnetic field of 0.6 T and 0.05 kN bias load was obtained for the directionally solidified $Ni_{50}Mn_{30}Ga_{20}$ alloy.

REFERENCES

1. Chernenko, V.A.; Cesari, E.; KoKorin, V.V. & Vitenko, I.N., The development of new ferromagnetic shape memory alloys in Ni-Mn-Ga system. *Scripta Met. Mater.*, 1995, **33** (8), 1239.
doi: 10.1016/0956-716X(95)00370-B
2. Ullakko, K.; Huang, J.K.; Kantner, C.; O' Handley, R.C. & Kokorin, V.V. Large magnetic field induced strains in Ni_2MnGa single crystals. *Appl. Phys. Lett.*, 1996, **69** (13), 1966.
doi: 10.1063/1.117637
3. Murray, S.J.; Marioni, M.A.; Kukla, A.M.; Robinson, J.; O'Handley, R.C. & Allen, S.M. Large field induced strain in single crystalline Ni–Mn–Ga ferromagnetic shape memory alloy. *J. Appl. Phys.*, 2000, **87** (9), 5774.
doi: 10.1063/1.372518
4. Soderberg, O.; Ge, Y.; Sozinov, A.; Hannula, S.-P. & Lindros, V.K. Recent breakthrough development of the magnetic shape memory effect in Ni-Mn-Ga alloys. *Smart Mater. Struct.*, 2005, **14**, S223.
doi: 10.1088/0964-1726/14/5/009
5. Sozinov, A.; Likhachev, A.A.; Lanska, N. & Ullakko, K. Giant magnetic field induced strains in NiMnGa seven layered martensite phase. *Appl. Phys. Lett.*, 2002, **80**(10), 1746.
doi: 10.1063/1.1458075
6. O'Handley, R.C.; Murray, S.J.; Marioni, M.; Nembach, H. & Allen, S.M. Phenomenology of giant magnetic-field-induced strain in ferromagnetic shape-memory materials. *J. Appl. Phys.*, 2000, **87**(9), 4712.
doi: 10.1063/1.373136
7. O'Handley, R.C. Model for strain and magnetization in magnetic shape-memory alloys. *J. Appl. Phys.*, 1998, **83** (6), 3263.

doi: 10.1063/1.367094
8. Wuttig, M.; Li, J. & Carciunescu, C. A new ferromagnetic shape memory alloy system. *Scripta Mater.*, 2001, **44**, 2393.
doi: 10.1016/S1359-6462(01)00939-3
9. Wuttig, M.; Liu, L.; Tsuchiya, K. & James, R.D. Occurrence of ferromagnetic shape memory alloys. *Appl. Phys.*, 2000, **87**(9), 4707.
doi: 10.1063/1.373135
10. Murray, S.J.; O'Handley, R.C. & Allen, S.M., Model for discontinuous actuation of ferromagnetic shape memory alloy under stress. *J. Appl. Phys.*, 2001, **89**(2),1295.
doi: 10.1063/1.1285867
11. Heczko, O.; Straka, L.; Lanska, N.; Ullakko, K. & Enkovaara, J. Temperature dependence of magnetic anisotropy in Ni-Mn-Ga alloys exhibiting giant field induced strains. *J. Appl. Phys.*, 2001, **91**, 8228.
doi: 10.1063/1.1453944
12. Likhachev, A.A. & Ullakko, K. Magnetic field controlled twin boundaries motion and giant magneto-mechanical effects in Ni-Mn-Ga shape memory alloys. *Phys. Lett. A*, 2000, **275**,142.
doi: 10.1016/S0375-9601(00)00561-2
13. Kakeshita, T. & Ullakko, K. Giant magnetostriction in ferromagnetic shape-memory alloys. *MRS Bulletin*, 2002,**12**, 105. doi: 10.1557/mrs2002.45
14. Pons, J.; Cesari, E.; Segui, C.; Masdeu, F. & Santamarta, R. Ferromagnetic shape memory alloys: Alternatives to Ni–Mn–Ga. *Mater. Sci. Eng. A*, 2008, **481-482**, 57.
doi: 10.1016/j.msea.2007.02.152
15. Chernenko, V.A. & Besseghini, S. Ferromagnetic shape memory alloys: Scientific and applied aspects. *Sensors Actuators A*, 2008, **142**, 542.
doi: 10.1016/j.sna.2007.05.023
16. Wilson, S.A.; Jourdain, R.P.J.; Zhang, Q.; Dorey, R.A. New materials for micro-scale sensors and actuators an engineering review. *Mat. Sci. Engg. R*, 2007, **56**,1.
doi: 10.1016/j.mser.2007.03.001
17. Webster, P.J.; Ziebeck, K.R.A.; Town, S.L. & Peak, M.S. Magnetic order and phase transformation in Ni_2MnGa. *Philos. Mag. B*, 1984, **49**, 295.
doi: 10.1080/13642817408246515
18. Chernenko, V.A. Compositional instability of β-phase in Ni-Mn-Ga alloys. *Scripta Mater.*, 1999, **40**, 523.
doi: 10.1016/S1359-6462(98)00494-1
19. Martynov, V.V. & Kokorin, V.V. The crystal structure of thermally- and stress-induced martensites in Ni_2MnGa single crystals. *J. Phys. III France*, 1992, **2**, 739.
doi: 10.1051/jp3:1992155
20. Pons, J.; Chernenko, V.A.; Santamarta, R. & Cesari. E. Crystal structure of martensitic phases in Ni-Mn-Ga shape memory alloys. *Acta Mater.*, 2000, **48**, 3027.
doi: 10.1016/S1359-6454(00)00130-0
21. Han, M.; Bennett, J.C.; Gharghouri, M.A.; Chen, J.; Hyatt, C.V. & Mailman, N. Microstructure characterization of the non-modulated martensite in Ni–Mn–Ga alloy. *Mater. Charac.*, 2008, **59**, 764.
doi: 10.1016/j.matchar.2007.06.010
22. Jin, X.; Marioni, M.; Bono, D.; Allen, S.M. & O'Handley, R.C. Empirical mapping of Ni-Mn-Ga properties with composition and valence electron concentration. *J. Appl. Phys.*, 2002, **91**, 8222.
doi: 10.1063/1.1453943
23. Richard, M.; Feuchtwanger, J.; Schlagel, D.; Lograsso, T.; Allen, S.M. & O'Handley, R.C. Crystal structure and transformation behavior of Ni–Mn–Ga martensites. *Scripta Mater.*, 2006, **54**, 1797.
doi: 10.1016/j.scriptamat.2006.01.033
24. Webster, P.J.; Ziebeck, K.R.A.; Town, S.L. & Peak, M.S. Magnetic order and phase transformation in Ni_2MnGa. *Philos. Mag. B*, 1984, **49**, 295.
doi: 10.1080/13642817408246515
25. Enkovaara, J.; Heczko, O.; Ayuela, A. & Nieminen, R.M. Coexistence of ferro- and antiferromagnetic order in Mn-doped Ni_2MnGa. *Phys. Rev. B*, 2003, **67**, 212405.
doi: 10.1103/PhysRevB.67.212405
26. Tickle, R. & James, R.D. Magnetic and magnetomechanical properties of Ni_2MnGa. *J. Magn. Magn. Mater.*, 1999, **195**, 627.
doi: 10.1016/S0304-8853(99)00292-9
27. Heczko, O.; Sozinov, A. & Ullakko, K. Giant field-induced reversible strain in magnetic shape memory NiMnGa alloy. *IEEE Trans. Magn.*, 2000, **36**, 3266.
doi: 10.1109/20.908764
28. Shanina, B.D.; Konchits, A.A.; Kolesnik, S.P.; Gavriljuk, V.G.; Glavastskij, I.N.; Glavatska, N.I.; Sodergerg, O.; Lindroos, V.K. & Foct, J. Ferromagnetic resonance in non-stoichiometric $Ni_{1-x-y}Mn_xGa_y$. *J. Magn. Magn. Mater.*, 2001, **237**, 309.
doi: 10.1016/S0304-8853(01)00508-X
29. Eshelman, M.A.; Seetharaman, V. & Trivedi, R. Cellular spacings - I. Steady-state growth. *Acta Metall.*, 1988, **36**, 1165.
doi: 10.1016/0001-6160(88)90169-1
30. Chalmers, B. Principles of solidification. Wiley press, New York, 1964.
31. Flemings, M.C. Solidification processing. McGraw Hill, New York, 1974.
32. Kurz, W. & Fisher, D.J. Fundamental of solidification. Trans. Tech. Publ., Aedermannsdorf, Switzerland, 1986.
33. Jie, W. Solute redistribution and segregation in solidification process. *Sci. Tech. Adv. Mater.*, 2001, **2**, 29.
doi: 10.1016/S1468-6996(01)00022-5
34. Gaitzsch, U.; Roth, S.; Rellinghaus, B. & Schultz, L. Adjusting the crystal structure of NiMnGa shape memory ferromagnets. *J. Magn. Magn. Mater.*, 2006, **305**, 275.
doi: 10.1016/j.jmmm.2006.01.017
35. Heczko, O. & Straka, L. Compositional dependence of structure, magnetization and magnetic anisotropy in Ni–Mn–Ga magnetic shape memory alloys. *J. Magn. Magn. Mater.*, 2004, **272**, 2045.
doi: 10.1016/j.jmmm.2003.12.819
36. Maki, T. Shape memory materials: Ferrous shape memory alloys, Cambridge university press, UK, 1998, 122p.
37. Kajiwara, S. Characteristic features of shape memory effect and related transformation behavior in Fe-based

alloys. *Mater. Sci. Eng. A*, 1999, **273-275**, 67.
doi: 10.1016/S0921-5093(99)00290-7

38. Hamilton, R.F.; Dilibal, S.; Sehitoglu, H. & Maier, H.J. Inter-martensite strain evolution in NiMnGa single crystals. *Acta Mater.*, 2008, **56**(10), 2231.
doi: 10.1016/j.actamat.2008.01.007
39. Wang, Y.D.; Brown, D.W.; Choo, H.; Liaw, P.K.; Cong, D.Y.; Benson, M.L. & Zuo, L. Experimental evidence of stress-field-induced selection of variants in Ni-Mn-Ga ferromagnetic shape-memory alloys. *Phys. Rev. B*, 2007, **75**, 174404.
doi: 10.1103/PhysRevB.75.174404
40. Okamoto, N.; Fukuda, T.; Kakeshita, T. & Takeuchi, T. Magnetocrystalline anisotropy constant and twinning stress in martensite phase of Ni–Mn–Ga. *Mater. Sci. Eng. A*, 2006, **438–440**, 948.
doi: 10.1016/j.msea.2006.02.121

ACKNOWLEDGEMENT

The authors are thankful to Defence Research & Development Organisation, India for the financial support through a project. Authors express their thanks to the Director, Defence Metallurgical Research Laboratory, Hyderabad for his constant encouragement and permission to publish these results.

CONTRIBUTORS

Dr R.K. Singh received his BTech (Metallurgical Engineering) from the Indian Institute of Technology Roorkee, in 2002. And MTech and PhD (Metallurgy) from Indian Institute of Technology, Banaras Hindu University, Varanasi, in 2006 and 2012, respectively. Currently working as a Scientist at Defence Metallurgical Research Laboratory, Hyderabad, India. His research area includes : Development of ferromagnetic shape memory alloys, Ni-Ti based shape memory alloys, Sm-Co based permanent magnets.

Dr M. Manivel Raja received his BSc and MSc in Physics from the Madurai-Kamaraj University, Madurai, India, in 1989 and 1991 respectively and PhD (Nuclear Physics) from the University of Madras, Chennai, India in 1997. Currently working as a Scientist-F at Defence Metallurgical Research Laboratory, Hyderabad, India. He is conducting research on magnetism and magnetic materials for more than 15 years. He has published more than 100 research papers in reputed international journals.

Dr Partha Ghosal has received his PhD from Indian Institute of Technology, Banaras Hindu University, in 1996. Currently, working as Head, Microscopy Group in the at Defence Metallurgical Research Laboratory, Hyderabad. He is working in the area of advanced characterisation techniques, along with SEM, EBSD, TEM and HRTEM. This includes *in-situ* mechanical testing and heating experiments of nano and advanced materials inside electron microscopes. Extensive electron microscopic works on Ti and W based alloys, nano-materials and nano composites is also carried out by him and in the scope of his interest.

Dr R.P. Mathur received his BE from Rajasthan University, Jaipur, in 1982 and MTech from Indian Institute of Technology, Kanpur, in 1991. Received his PhD from Indian Institute of Technology, Rorkee, in 2008. Currently working as a Scientist at Defence Metallurgical Research Laboratory, Hyderabad, India. He has published about 25 research papers in reputed international journals and more than 30 papers in national/ international conference proceedings. His areas of research interest include: Amorphous alloys, nano structured soft/hard magnetic materials, rare earth permanent magnets, functional materials such as shape memory alloys.